

# **Residual Stress Distributions around Indentations and Scratches in Polycrystalline $\text{Al}_2\text{O}_3$ and $\text{Al}_2\text{O}_3/\text{SiC}$ Nanocomposites Measured using Fluorescence Probes**

**H.Z. Wu\***, **S. G. Roberts\*\*** and **B. Derby\*\*\***

\*IPTME, Loughborough University, Leicester, LE11 3TU, UK

\*\*Department of Materials, University of Oxford, Oxford OX1 3PH, UK

\*\*\*School of Materials, University of Manchester, Grosvenor St., Manchester, M1 7HS UK

## **Abstract**

We report a study of the residual stress state around indentations and single point scratches in polycrystalline alumina and alumina/SiC nanocomposites using  $\text{Cr}^{3+}$  fluorescence piezospectroscopy. The alumina specimens displayed residual stress levels up to 550 MPa whereas the nanocomposite specimens had maximum stress levels close to 2 GPa. These stress levels are consistent with those obtained using other experimental techniques. The spatial variation of this stress is shown to be consistent with simple elastic/plastic models of indentation. The broadening of the peaks in the fluorescence spectra is used to estimate the density of dislocations in the plastically deformed region below indentations and scratches. Our results indicate a greater depth of deformation around indents and scratches in the nanocomposites when compared with the alumina surfaces. The inferred dislocation densities and the depth of the deformed region beneath the alumina and nanocomposite surfaces are shown to be consistent with those of ground surfaces reported in earlier studies.

# 1 Introduction

Alumina/silicon carbide nanocomposites (alumina polycrystals containing small fractions of sub-micron sized SiC particles) can show large increments of strength above polycrystalline alumina samples with equivalent grain size; any increase in strength is not accompanied by any significant increase in material toughness [1,2,3,4]. A number of workers have proposed that the surface properties of alumina/SiC nanocomposites are the key to their enhanced strength, in particular near-surface in-plane compressive stresses introduced by surface finishing operations.

Recent work has found intriguing differences between the surface behaviour of alumina polycrystals and alumina/SiC nanocomposites. Sternitzke *et al* [5] first reported a quantitative difference in the sub-surface damage between alumina and alumina/SiC nanocomposites after grinding and polishing. Other studies also reported enhanced strength in these nanocomposites after surface grinding [1] and a much superior polished surface with suppressed grain pull-out [6,7]. Wu *et al* showed [8] that grinding the surface of alumina/SiC nanocomposites with a coarse diamond grit wheel resulted in a 4-point bend strength of ~400 MPa, whereas similarly ground alumina specimens had a strength of ~300 MPa. The enhanced strength of the nanocomposites was shown to be associated with a large compressive surface stress induced by surface grinding, while such a magnitude of residual stress was not present in the alumina after identical surface treatment. A more detailed study of the surface stress state, and the sub-surface dislocation structure after deformation, found that the nanocomposite material showed a significantly greater dislocation density beneath ground and polished surfaces, compared to identically-treated polycrystalline alumina [9,10,11].

In order to investigate further the influence of surface grinding on the mechanical behaviour of alumina and alumina/SiC nanocomposites, we have undertaken a study of the deformation around single point indentations and simple scratch grooves. Such surface deformation can be taken as a model for the processes occurring around individual grit particles during grinding. The mechanisms of deformation around indentations in ceramics and brittle materials have been the subject of considerable research in the past. It is now generally accepted that even in highly brittle materials there is a region of plastic deformation immediately below the indentation [12]; this is shown schematically in figure 1. During indentation an elastic stress field is generated, of radial compression and tangential tension, extending into the material outside the plastic zone, the magnitude of which decays with distance,  $r$ , from the centre of the plastic zone as  $1/r^2$  [13,14]. The tensile components of this stress field can lead to the nucleation of radial and median cracks on loading. The magnitude of the residual elastic stress field after unloading varies as  $1/r^3$  from the contact point [14,15] (though it may be influenced by the presence of the crack systems illustrated in figure 1). The residual stress field close to the surface has a tension component normal to the surface, which may lead to the nucleation of lateral cracks. For a sliding indentation, there is as yet no model that can completely describe the elastic plastic stress fields under the indenter. An extension of Yoffe's model of static indentation to sliding contacts has been reported [16], though further validation is needed.

Conventional methods of residual stress measurement, e.g. X-ray diffraction or surface curvature changes, measure the residual stress averaged over a considerable region of material. In order to obtain a high resolution local picture of the residual stress state on the surface close to scratches and indentations, we have used the  $\text{Cr}^{3+}$  fluorescence spectra obtained from natural concentrations of Cr impurities within alumina crystals. Grabner [17]

first described the relationship found between the measured line shift in  $\text{Cr}^{3+}$  fluorescence and the local stress state. Ma and Clarke developed this analysis for a more general case to relate the mean line shift to the local stress tensor [18]. They also presented an analysis of the broadening of the fluorescence peak to determine the mean stress distribution in an illuminated area. Thus, by using an optical microscope of sufficient resolution fitted with an appropriate spectrometer, it is possible to determine the surface stress within alumina specimens with a lateral spatial resolution of about 1  $\mu\text{m}$  and over a sampled depth slightly greater than this [19].

## **2 Experimental Procedure**

The materials used in this study consist of a polycrystalline alumina (AKP53, Sumitomo Chemical Co., Tokyo, Japan) of mean grain size about 3  $\mu\text{m}$  and an alumina/SiC nanocomposite with a matrix of the AKP53 alumina containing 1%, 5%, and 10% by volume  $\alpha$ -SiC particles (UF 45, Lonza, Waldshut, Germany), with a mean particle diameter of 90 nm. Processing conditions were chosen to ensure that the nanocomposite and polycrystalline alumina had equivalent mean grain size. The processing routes used have been described in detail elsewhere [3,8]. All nanocomposite samples were hot pressed at 1650° C for 1 hour under a pressure of 20 MPa in argon. The alumina samples were hot pressed at 1500° C for 1 hour under same pressure. All nanocomposites and alumina ceramics achieved full density after fabrication.

The hot-pressed ceramic discs, with a thickness of about 5 mm, were ground with an epoxy resin bonded diamond wheel (grit size 150  $\mu\text{m}$ ) to remove the top surface on both sides, producing a final specimen thickness of about 3 mm. Specimens for indentation and scratch

experiments were cut directly from the ground discs with a diamond saw and the ground surfaces were lapped and polished using a series of diamond grits of 25  $\mu\text{m}$ , 8  $\mu\text{m}$ , 3  $\mu\text{m}$  and 1  $\mu\text{m}$  grit size. Each step of the polishing sequence was performed for sufficient time to eliminate all surface damage induced by the previous polishing step. Full details of this surface finishing process have been presented elsewhere [8,9].

## **2.1 Single Point Indentation and Scratch Tests**

All indentation and scratch tests were carried out on surfaces polished to a 1  $\mu\text{m}$  diamond finish. A microindenter (Matsuzawa MHT1, Tokyo, Japan) was used to produce indentations on the surface of the alumina and alumina/silicon carbide nanocomposites using a square pyramid diamond with tip included angle of  $136^\circ$  (Vickers profile). Indentation loads in the range of 0.5 – 10 N were used with a holding time of 15 s at maximum load for each indentation experiment.

Single-point scratch tests were carried out by traversing the specimens beneath a loaded conical diamond indenter ( $120^\circ$  tip included angle) by means of an electric motor and gearbox driving a stage micrometer. The traverse speed was  $0.05 \text{ mms}^{-1}$ . The normal loads used were in the range 0.5 – 10 N. The accuracy of the applied load is approximately  $\pm 0.02\text{N}$ ; however, each test series was performed using the same arm balance conditions, hence within each test series the load on the specimens was identical.

## **2.2 Fluorescence spectra measurement**

$\text{Cr}^{3+}$  fluorescence spectra were obtained using a Raman microprobe, Renshaw system 1000 (Renishaw, Wootton-under-Edge, UK), mounted on an optical microscope and adapted for

Cr<sup>3+</sup> fluorescence measurements, using the 632.8 nm red line of a 15 mW He-Ne laser with an intensity of about 1.0 mW. This level of laser beam intensity has been found to cause minimum shift in the wavenumbers of the fluorescence lines due to heating effects [19]. Measurements were made using a ×40 microscope objective lens with a numerical aperture of 0.65, which gives an approximate beam diameter on the specimen surface of about 2 μm. All of the calibrations and tests were carried out in a controlled environment at constant temperature of 22° ± 2° C.

For each measurement, a region of interest was selected using the optical microscope with white light and focused on to the top surface plane by adjusting the height of the sample stage. A series of fluorescence measurements was carried out along the required directions in these selected regions. The probe position was manually monitored by a micrometer gauge on the sample stage. To ensure the focal plane of the laser was on the specimen surface, the probe was refocused at each test position. The fluorescence lines were collected using a scanning spectrometer grating with a step of 0.2 cm<sup>-1</sup> integrating over 0.5 s intervals. The characteristic neon line at 14431 cm<sup>-1</sup> was used as a frequency standard. The collected data were subsequently analysed with curve-fitting algorithms included in the SpectraCalc software package (Galactic Industries Corp., Salem, NH, USA). The line position and width were identified by simultaneously fitting the R1 and R2 peaks with Gaussian and Lorentzian functions. Curve fits were always obtained at a high level of confidence for all the spectra obtained from the scratches and indents. Repeating measurements for the same position on the surface showed that the standard deviation is small enough to be ignored. For all probe positions, therefore, only one measurement was made.

Fracture surfaces of each material tested, assumed to be stress-free, were used as reference zeros for the peak shift. The fluorescence line position on the fracture surface was an average

of 30 random measurements on both the alumina and the nanocomposite. Shifts shown at any position near the indentation or scratch are therefore taken as an indication of the residual stress level after deformation.

### 3 Analysis of fluorescence line shift and broadening

The  $\text{Cr}^{3+}$  fluorescence measurements show significant levels of residual stress close to the scratches and indentations (see section 4). These residual stresses are caused by the superposition of stress fields from a number of independent mechanisms (where  $\langle\sigma\rangle$  indicates a stress tensor):

$$\langle\sigma\rangle = \langle\sigma\rangle^{ATE} + \langle\sigma\rangle^{MTE} + \langle\sigma\rangle^{DL} + \langle\sigma\rangle^{MC} + \langle\sigma\rangle^{LE} \quad (1)$$

- i.  $\langle\sigma\rangle^{ATE}$  is caused by the influence of the anisotropic thermal expansion of the hexagonal  $\alpha$ -alumina phase on the polycrystalline aggregate.
- ii.  $\langle\sigma\rangle^{MTE}$  is the stress from the mismatch in thermal expansion coefficient between the alumina and SiC phases.
- iii.  $\langle\sigma\rangle^{DL}$  represents the stress field around dislocations.
- iv.  $\langle\sigma\rangle^{MC}$  represents the perturbations to the stress field introduced by the presence of microcracks.
- v.  $\langle\sigma\rangle^{LE}$  is a large scale elastic stress.

The approach of Ma and Clarke [18] can be used to assess the contributions of these residual stresses to the shift and broadening of the fluorescence spectrum. For the purposes of this discussion we will consider alumina to be an elastically isotropic material. This assumption should be reasonable because despite its trigonal symmetry,  $\alpha\text{-Al}_2\text{O}_3$  has very similar elastic

stiffness values along the principal crystallographic directions, i.e.  $c_{11} = c_{22} = 497$  GPa,  $c_{33} = 498$  GPa, and in the principal planes, i.e.  $c_{12} = 164$  GPa and  $c_{13} = 111$  GPa [20]. In a uniformly stressed volume of material probed for the  $\text{Cr}^{3+}$  fluorescence, the shift in the fluorescence peak is given by

$$\Delta\mu = (\sigma_{xx} + \sigma_{yy})\Pi_a + \sigma_{zz}\Pi_c \quad (2)$$

where  $\mu$  is the wavenumber of the fluorescence line and  $\Pi_a$  and  $\Pi_c$  are the piezospectroscopic coefficients in the basal plane and along the z-axis of the alumina respectively. Note that only the direct stresses  $\sigma_{xx}$ ,  $\sigma_{yy}$  and  $\sigma_{zz}$  contribute to the piezospectroscopic effect. Within an inhomogeneous stress field, the shift of the fluorescence peak can be calculated by integrating over all wavenumbers generated in the probed region:

$$\overline{\Delta\mu} = \int \Delta\mu w(\Delta\mu) d\Delta\mu \quad (3)$$

and the corresponding peak broadening is hence

$$\langle \Delta\mu^2 \rangle = \int \Delta\mu^2 w(\Delta\mu) d\Delta\mu - \overline{\Delta\mu}^2 \quad (4)$$

where  $w(\Delta\mu)$  is a weighting function.

Given the relatively large volume of material illuminated, and the condition of stress equilibrium, we expect that the effect on the shift in the peak position of mechanisms i – iv to be negligible. Thus it is only the large scale elastic stress distribution that is expected to influence the *shift* in the fluorescence peak. The *broadening* of each spectrum is always compared with that of a presumed stress-free state of the same material obtained from a freshly fractured surface. Thus, the first two terms,  $\langle \sigma \rangle^{\text{ATE}}$  and  $\langle \sigma \rangle^{\text{MTE}}$ , can be excluded.



Any change in the broadening of the spectra can only come from stresses due to dislocations and subsurface cracks inside the probed volume. The weighting function in equation 4 determines the extent of broadening, which is in turn a representation of the range in magnitude of the internal residual stress distribution and its spatial extent referred to the scale of the illuminated volume. If there is a significant population of dislocations in the illuminated volume, the contribution from their stress fields will dominate the broadening relation; because of the far lower density of cracks, any stress concentration around the crack tips can make only a minor contribution.

In order to consider the influence of dislocation density on the broadening of the fluorescence signal, the stress field around each dislocation must be known. We approximate the elastic stress field around the dislocations to that of dislocations in a uniform, isotropic elastic medium. Since the shear stress terms do not contribute to the fluorescence shift, there can be no contribution to the shift or broadening from screw dislocations. The major stress components around a single edge dislocation in an elastically isotropic medium are as follows [21]:

$$\sigma_{x'x'} = -\frac{Gb}{2\pi(1-\nu)r} \sin \theta (2 + \cos 2\theta) \quad (5a)$$

$$\sigma_{y'y'} = \frac{Gb}{2\pi(1-\nu)r} \sin \theta \cos 2\theta \quad (5b)$$

$$\sigma_{z'z'} = -\frac{Gb}{\pi(1-\nu)r} \nu \sin \theta \quad (5c)$$

where  $G$  is the shear modulus,  $b$  the Burgers vector,  $\nu$  the Poisson's ratio; the axes  $x'$ ,  $y'$  and  $z'$  define a reference frame with  $z'$  parallel to the dislocation line and  $b$  acting along the  $x'$

direction. For simplicity we take this as the stress distribution around dislocations in the  $\alpha$ -alumina crystal structure. We make a further simplification and assume that all dislocations are of edge character and lie in the basal plane. This is in keeping with our observations that although non-basal dislocations do exist in deformed alumina, basal plane dislocations dominate [22]. Hence, the shift of the fluorescence lines will be given by

$$\Delta\mu = (\sigma_{x'x'} + \sigma_{z'z'})\Pi_a + \sigma_{y'y'}\Pi_c \quad (6)$$

Considering the stress field around a single dislocation in isolation, the weighting function is related to the volume of material contributing to a given spectral wavenumber, because the intensity of the fluorescence is determined solely by the concentration of  $\text{Cr}^{3+}$  ions, which should be distributed homogeneously within the alumina. For a single dislocation, the relative contribution to the shift at each position is integrated over the volume between an inner and outer cut-off radius ( $r_i$  and  $r_o$ ), with the mean spectral shift contributed by each dislocation given by:

$$\overline{\Delta\mu} = \frac{Gb}{2\pi(1-\nu)} \int_0^{2\pi} \int_{r_i}^{r_o} \left\{ (\Pi_c - \Pi_a) \frac{\sin\theta \cos 2\theta}{r} - 2(1+\nu)\Pi_a \frac{\sin\theta}{r} \right\} \frac{rdrd\theta}{\pi(r_o^2 - r_i^2)} = 0 \quad (7)$$

The broadening relation is thus:

$$\begin{aligned} \langle \Delta\mu^2 \rangle = & \left( \frac{Gb}{2\pi(1-\nu)} \right)^2 \int_0^{2\pi} \int_{r_i}^{r_o} \left\{ (\Pi_c - \Pi_a)^2 \frac{\sin^2\theta \cos^2 2\theta}{r^2} \right. \\ & \left. - 4(1+\nu)\Pi_a(\Pi_c - \Pi_a) \frac{\sin^2\theta \cos 2\theta}{r^2} + 4(1+\nu)^2 \Pi_a^2 \frac{\sin^2\theta}{r^2} \right\} \frac{rdrd\theta}{\pi(r_o^2 - r_i^2)} \end{aligned} \quad (8)$$

On integration this results in

$$\begin{aligned} \langle \Delta \mu^2 \rangle = & \frac{G^2 b^2}{4\pi^3 (1-\nu)^2 (r_o^2 - r_i^2)} \left\{ (\Pi_c - \Pi_a)^2 \frac{\pi}{2} + 4(1+\nu) \Pi_a (\Pi_c - \Pi_a) \frac{\pi}{2} \right. \\ & \left. + 4(1+\nu)^2 \Pi_a^2 \pi \right\} \ln \left( \frac{r_o}{r_i} \right) \end{aligned} \quad (9)$$

If the dislocations are uniformly distributed, the outer cut-off radius is related to dislocation density,  $\rho$ , with  $\rho = 1/\pi r_o^2$ . Then  $r_i \ll r_o$  and can be approximated to the Burgers vector,  $r_i = b$ . From this we can derive a measure of the line broadening as a function of dislocation density with:

$$\begin{aligned} \sqrt{\langle \Delta \mu^2 \rangle} &= \frac{Gb \sqrt{\rho \ln(1/b\sqrt{\pi\rho})}}{2\sqrt{\pi}(1-\nu)} \left\{ (\Pi_c - \Pi_a)^2 \frac{1}{2} + 2(1+\nu) \Pi_a (\Pi_c - \Pi_a) + 4(1+\nu)^2 \Pi_a^2 \right\}^{1/2} \\ &= \frac{Gb \sqrt{\rho \ln(1/b\sqrt{\pi\rho})}}{2\sqrt{2\pi}(1-\nu)} \left\{ (5+12\nu+2\nu^2) \Pi_a^2 + 2(1+2\nu) \Pi_a \Pi_c + \Pi_c^2 \right\}^{1/2} \end{aligned} \quad (10a)$$

or for simplicity

$$\sqrt{\langle \Delta \mu^2 \rangle} = KF(\rho) \quad (10b)$$

$$\text{with} \quad K = \frac{Gb}{2\sqrt{2\pi}(1-\nu)} \left\{ (5+12\nu+2\nu^2) \Pi_a^2 + 2(1+2\nu) \Pi_a \Pi_c + \Pi_c^2 \right\}^{1/2} \quad (10c)$$

$$\text{and} \quad F(\rho) = \sqrt{\rho \ln(1/b\sqrt{\pi\rho})} \quad (10d)$$

For alumina the values of the required physical constants are:  $G = 150$  GPa,  $\nu = 0.24$ ,  $b = 0.476$  nm for the  $1/3\langle 2\bar{1}\bar{1}0 \rangle$  Burgers vector,  $\Pi_a = 2.7 \text{ cm}^{-1}\text{GPa}^{-1}$  and  $\Pi_c = 2.15 \text{ cm}^{-1}\text{GPa}^{-1}$  [23]. Using these data, the predicted line broadening as a function of dislocation density can be calculated and is presented in figure 2a.

Note that equation 10 assumes the fluorescence to come from a volume of material containing a constant dislocation density. During fluorescence measurements the signal originates from an illuminated volume determined by the collection optics of the system. Thus there is likely to be a non-constant density of dislocations within the illuminated volume and this will also influence the broadening of the fluorescence signal. Ma and Clarke [18] have determined the volume illuminated using a modified confocal microscope to be approximated by a two-dimensional Gaussian function. In our instrument, with a focussed spot on the surface, the illuminated volume may be equivalent to half such a function. However, for simplicity in analysis we assume the illuminated volume to be represented by a cylinder of radius  $a$  and depth  $l$ . In an earlier study of residual stress in alumina and nanocomposites, it was assumed that the deformation that occurs after grinding and machining was concentrated in a zone of fixed depth,  $h$ , beneath the surface and that this zone had a constant dislocation density [9]. Such a step function of dislocation density is very easy to model considering the weight function approach used in equation 4. In this case equation 10 is written

$$\sqrt{\langle \Delta\mu^2 \rangle} = K\sqrt{f}F(\rho) \quad (11)$$

where  $f$  is the fraction of the illuminated volume that contains the surface region of constant dislocation density.

For our simplified model of a cylindrical illuminated volume,  $f = h/l$ . The physical meaning of equation (11) is that the broadening of the fluorescence is determined both by the depth of the deformed layer (if this is less than the illuminated depth) and by its dislocation density. Figure 2b indicates the inter-relation between the extent of peak broadening, dislocation density and thickness of the deformed zone. The simulation results show that the dislocation density is a significant contribution to the broadening of the fluorescence peak when the dislocation density in the illuminated volume is larger than  $\sim 10^{14} \text{ m}^{-2}$  (see fig. 2a). With a

dislocation density larger than  $\sim 10^{14} \text{ m}^{-2}$ , the ratio of the depth of the deformed layer to that of the laser illumination has a significant influence on the broadening level. However, when the dislocation density is less than  $\sim 10^{14} \text{ m}^{-2}$  inside the deformed layer, the deformation depth has little influence on the peak broadening.

## 4 Experimental Results and Discussion

Typical examples of the resolved shift and broadening (FWHM) for R1 and R2 fluorescence lines across the indentations and scratches in alumina and the nanocomposites are shown in figure 3 and figure 4. A load of 3N was used in both cases. The origin on the horizontal axis represents the centre of the indentation or scratch, and the negative and positive numbers indicate respectively the distance (in  $\mu\text{m}$ ) away from the central position on left and right hand side relative to the indentation or scratch centre. Indentation and scratching produce similar shift and line broadening effects are found around indentations and scratches. There is considerable difference in the observed behaviour between the alumina and the nanocomposite specimens, but there was little difference observed between the behaviour of the nanocomposites with 1%, 5% and 10% SiC.

In all specimens the measured line broadening is a maximum at the indentation or scratch centre and decays monotonically to the reference value over about 100  $\mu\text{m}$ . The broadening is considerably greater in the nanocomposites than in the polycrystalline alumina.

A more complex behaviour is seen with the measured line shift, with different behaviour found in the alumina and nanocomposites. The shift is greater in the nanocomposites and so its trend with distance from the indentation centre is easier to determine. In the scratch (figure

4b) there is a minimum in the (negative) shift at the origin, rising to a maximum at 20  $\mu\text{m}$  and decaying to zero over 100 – 200  $\mu\text{m}$ . The central region showing the minimum is approximately the extent of the physical scratch, which is about 14  $\mu\text{m}$  as shown in figure 5. This behaviour is also seen around the indentation for the R1 shift (figure 3b) but the R2 shift appears to show a maximum at the origin. In both cases the distance from the centre for the decay to zero shift is slightly less than 100  $\mu\text{m}$ . Curiously, the monolithic alumina specimens appear to show both positive and negative shifts (figures 3a and 4a) but of much lower magnitude than in the nanocomposites and with a spatial extent of 20 – 30  $\mu\text{m}$ , which is approximately the size of the indentation or scratch.

The average level of residual biaxial stress at a specified position across the contact impression can be determined from the magnitude of the shift of the fluorescence line using equation 2 [18]. By using He and Clarke's [23] calibration, the piezospectroscopic coefficient  $\Pi$  for line R1 is 2/3 of  $(2\Pi_a + \Pi_c)$ , i.e. 5.06  $\text{cm}^{-1}/\text{GPa}$  for polycrystalline alumina. Table 1 shows the maximum biaxial compression stresses determined from the maximum shifts of the R1 line for alumina and the nanocomposites under different normal loads of indentation and scratching. For any given load, the maximum residual compressive stress in the alumina is no more than half of that measured in any of the nanocomposites; among the nanocomposites, no obvious differences are observed with variation in SiC content in the range 1% to 10%.

In earlier work [8] we studied the effects of surface damage on the minimum load to produce ring-cracking around Hertzian indentations in alumina and nanocomposites. These data can be used to estimate the surface residual stresses [24]. Data were analysed by calculating the effects of biaxially compressed surface layers of varying stress level and depth on the results of the Hertzian tests. It was assumed that this residual stress was generated by a high

dislocation density generated by the grinding process. The best fit to the data was obtained with a residual stress of about 1500 MPa, which extended beneath the surface to a depth of 1 – 10  $\mu\text{m}$  (depending on grinding grit size) in the nanocomposites and for 0.1 – 1  $\mu\text{m}$  in alumina. This stress level is similar to the residual stress found in this study close to indentations and scratches on the nanocomposites, made with a 5 N or 10 N load, where we assume the depth of the dislocated layer to be greater than the penetration depth of the laser light.

For lower load scratches and indentations, we can make a similar hypothesis to that explored in [9]. The optical probe of the fluorescence microscope samples a fixed volume of material, thus if the plastic zone beneath the indenter is smaller than the sampled volume the mean compressive stress will be reduced compared to the case when the plastic zone fills the sample volume. This mechanism accounts for the apparent increase in residual stress with increasing load in the alumina specimens. It has been observed in previous work [9,10] that dislocation nucleation is considerably easier in nanocomposite microstructures than in monolithic alumina. Hence we can reasonably hypothesise a larger plastic zone beneath the indenter in the nanocomposite samples, explaining the larger measured stresses in Table 1 and the fact that the stress saturates around the 1000 – 1500 MPa level when, presumably, the depth of the plastic zone exceeds that of the sampled volume.

Figure 6 plots the biaxial stress on alumina and nanocomposite specimens, determined from fluorescence line shifts, as a function of distance from the centre of a scratch made with a 3 N load. The data from the alumina specimen (figure 6a) are very noisy and show no discernible trend. All the nanocomposite specimens behave similarly. The gradient on the logarithmic plot is consistent with the theoretical expectation that far-field elastic residual stresses decrease proportionally to  $r^{-3}$  [14]. These results are also consistent with a single plot of

hydrostatic stress, measured by fluorescence, as a function of distance from a 25 N indentation in a ruby single crystal reported by Banini et al [25]. The anomalous behaviour of the polycrystalline alumina and the deviation from the power-law behaviour in the nanocomposite specimens near to the scratch are probably caused by microcracking. The more severe cracking in the alumina is consistent with numerous reports on alumina/SiC nanocomposites that describe their greater resistance to grain boundary fracture compared to alumina [1-4].

The peak broadening data, measured as the maximum FWHM obtained from the centre of the indentation or scratch are given in Table 2. As was found with the fluorescence line shift data in Table 1, there is a significant difference between the behaviour of the alumina and nanocomposite specimens for any given load but all the nanocomposites showed very similar behaviour irrespective of SiC content. Further examination of the data suggests that the line broadening saturates with a FWHM value of about  $60 \text{ cm}^{-1}$ . If we assume that this saturation arises when the plastic zone depth exceeds the optical probe's sampling depth, then the dislocation density can be determined from equation 10 (plotted in figure 2a), giving a dislocation density of approximately  $10^{17} \text{ m}^{-2}$ . The lower values of line broadening seen in Table 2 do not represent lower dislocation densities in the plastic zone, rather they represent the fact that the sampled volume contains both the plastic zone and a region of only elastic deformation. Although equation 11 relates peak broadening to the fraction of the sampled volume occupied by the plastic zone, without precisely knowing the shape of the illuminated volume and the spatial variation of intensity, it is impossible to quantify the depth of any dislocation containing layer. In a study using TEM cross-sections [9], we have measured a maximum dislocated layer depth of about  $4 \text{ }\mu\text{m}$  under a single scratch generated with 1N normal load in alumina and about  $7 \text{ }\mu\text{m}$  for a similar scratch in a nanocomposite. This compares with a deformation zone depth of about  $1 \text{ }\mu\text{m}$  beneath a ground surface of alumina



and 3-10  $\mu\text{m}$  for a nanocomposite [9]. Our interpretations of the  $\text{Cr}^{3+}$  fluorescence data reported here are thus consistent with these earlier studies of dislocations beneath indentation, scratches and ground surfaces.

## 5 Conclusions

$\text{Cr}^{3+}$  fluorescence spectra can be used to analyse residual stress distributions in polycrystalline alumina and alumina/SiC nanocomposites. Changes in local stress on a scale smaller than sampling volume of the optical probe result in a broadening of the fluorescence line along with a shift in the line related to the mean hydrostatic stress of the sampled volume. The maximum compressive surface stress measured using fluorescence data increases with indentation load on polycrystalline alumina specimens to about 450 - 550 MPa. In the nanocomposites this stress reaches a steady level of around 1000 to 1700 MPa at loads  $\geq 3$  N irrespective of the volume fraction of SiC (in the range 1% - 10% SiC). The stress distribution distant from the contact line shows a power-law relation with distance from the centre line, with an exponent of about -3. This is consistent with elastic-plastic analysis indentations in the literature.

Inside the impressions left by indentation or scratching, there is no well defined trend in the line shift for all materials. However, a large degree of line broadening was observed inside the impressions in all the nanocomposite specimens, and a much smaller line broadening in the polycrystalline alumina. From an analysis of the available mechanisms for residual stress development in these materials, we conclude that the only mechanism that can explain the large extent of line broadening observed in the nanocomposite specimens is the presence of significant dislocation populations generated during indentation or scratch experiments. The much lower levels of both line shift and broadening found in the polycrystalline alumina

when compared with all the nanocomposite specimens is attributed to a much lower dislocation density in the alumina after single point deformation leading to indentation or scratch formation.

We further conclude that our results are consistent with earlier observations by many workers that surface finishing by grinding or polishing is an important aspect of the anomalously high strength levels found with alumina/SiC nanocomposites [1,5,8,9] and that their high strengths are associated with large surface residual compressive stresses resulting from a near-surface of plastically deformed region [9-11]. This plastically deformed layer is greater in depth for alumina/SiC nanocomposites than for polycrystalline alumina. Volume fractions of SiC as low as 1% are sufficient to produce this behaviour.

## **6 Acknowledgements**

We gratefully acknowledge the support of the EPSRC structural materials programme under grant GR/L95908. We would also like to acknowledge the assistance of Ms. R. Sinclair, Dr. S. Eichhorn and Dr. M. Montes in the Raman group of the School of Materials, University of Manchester.

## References

---

- 1 L.C. Stearn, J. Zhao, and M.P. Harmer, *J. Eur. Ceram. Soc.*, **10**, 473 (1992).
- 2 R.W. Davidge, R.J. Brook, F. Cambier, M. Poorteman, A. Leriche, D. O'Sullivan, S. Hampshire, and T. Kennedy, *Br. Ceram. Trans.*, **96**, 121 (1997).
- 3 L. Carroll, M. Sternitzke, and B. Derby, *Acta Metall. Mater.*, **44**, 4543 (1996).
- 4 M. Sternitzke, B. Derby, and R.J. Brook, *J. Am. Ceram. Soc.*, **81**, 41 (1998).
- 5 M. Sternitzke, E. Dupas, P. Twigg & B. Derby, *Acta Mater.*, **45**, 3963-3973 (1997).
- 6 A.J. Winn & R.I. Todd, *Brit. Ceram. Trans.*, **98**, 219 (1999).
- 7 H. Kara & S.G. Roberts, *J. Am. Ceram. Soc.*, **83**, 1219 (2000).
- 8 H.Z. Wu, C.W. Lawrence, S.G. Roberts, and B. Derby, *Acta Mater.*, **46**, 3839 (1998).
- 9 H.Z. Wu, S.G. Roberts & B. Derby, *Acta Mater.*, **49**, 507 (2001).
- 10 H.Z. Wu, B.J. Inkson & S.G. Roberts, *J. of Mic.*, **201**, 212 (2001).
- 11 B.K. Tanner, H.Z. WU, S.G. Roberts & T.P.A. Hase, *Phil. Mag. A*, **84**, 1219 (2004).
- 12 B. Lawn & R. Wilshaw, *J. Mater. Sci.*, **10**, 1049 (1975)
- 13 K.L. Johnson, *Contact Mechanics*. Cambridge University Press, Cambridge, 1985.
- 14 E.H. Yoffee, *Phil. Mag. A*, **46**, 617 (1982).
- 15 S.S. Chiang, D.B. Marshall & A.G. Evans, *J. Appl. Phys.*, **53**, 298, 1982
- 16 Y. Ahn, T.N. Farris & S. Chandrasekar, *Mech. Mater.*, **29**, 143 (1998)
- 17 L. Grabner, *J. Appl. Phys.*, **49**, 580 (1978).
- 18 Q. Ma and D.R. Clarke, *J. Am. Ceram. Soc.*, **76**, 1433 (1993).
- 19 R.B. Yaltee, M.C. Andrew & R.J. Young, *J. Mat. Sci.* **31**, 3349, (1996)

- 
- 20 J.B. Wachtman, Jr., D.G. Lam, Jr. & R.P. Stinchfield, *J. Res. NBA*, **64A**[3], 213 (1960)
- 21 J.P. Hirth and J. Lothe, *Theory of Dislocations*, Chichester, Wiley (1982)
- 22 H.Z. Wu, B.J. Inkson & S.G. Roberts, *J. Microsc.*, **201**, 212 (2001)
- 23 J. He & D.R. Clarke, *J. Am. Ceram. Soc.*, **78**, 1347 (1995).
- 24 S.G. Roberts, C.W. Lawrence, Y. Bisrat, P.D. Warren and D.A. Hills, *J. Am. Ceram. Soc.*, **82**, 1809 (1999)
- 25 G.K. Banini, M.M. Chaudhri, T. Smith and I.P. Hayward, *J. Phys D*, **34**, L122 (2001)

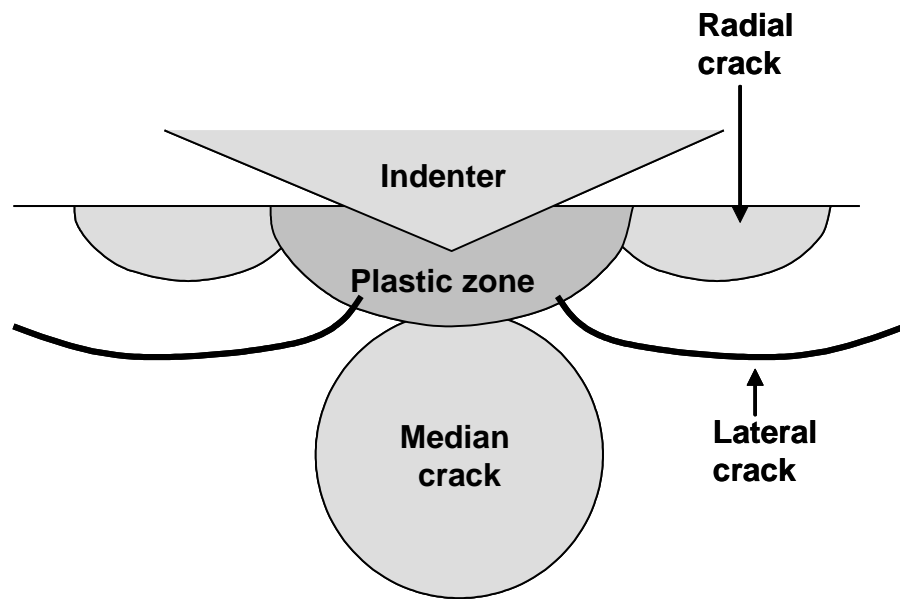
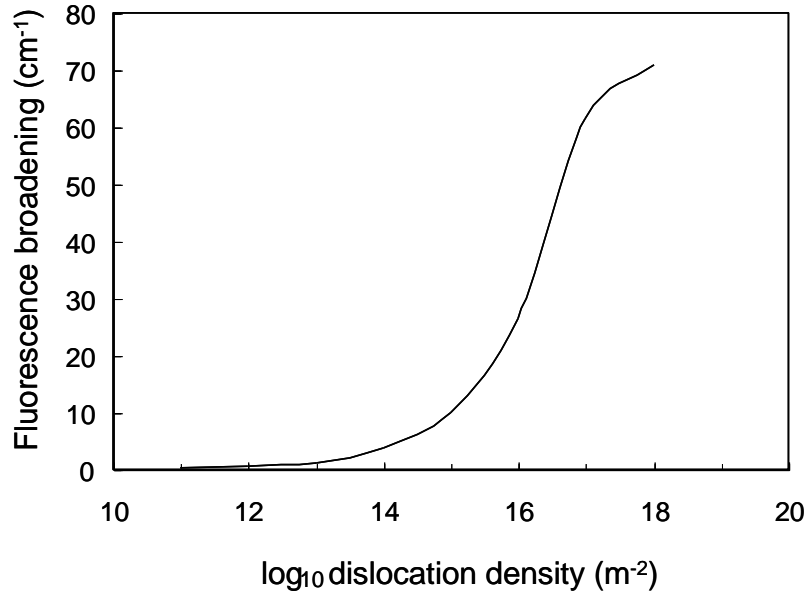
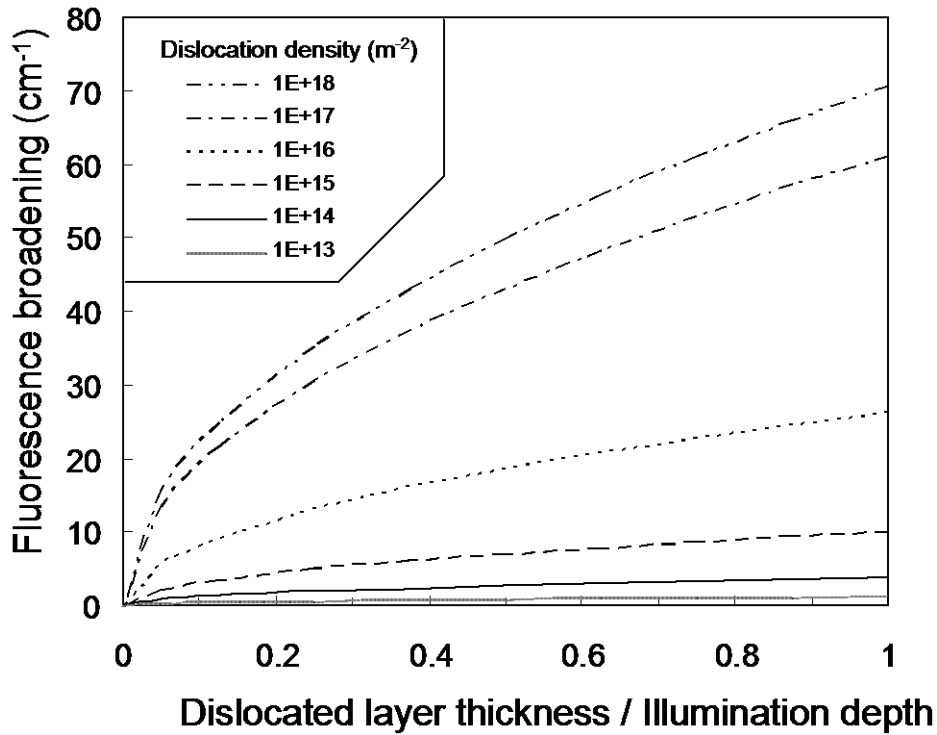


**Figure 1** Schematic showing the plastic zone beneath the indenter and the crack systems observed after unloading.



a)

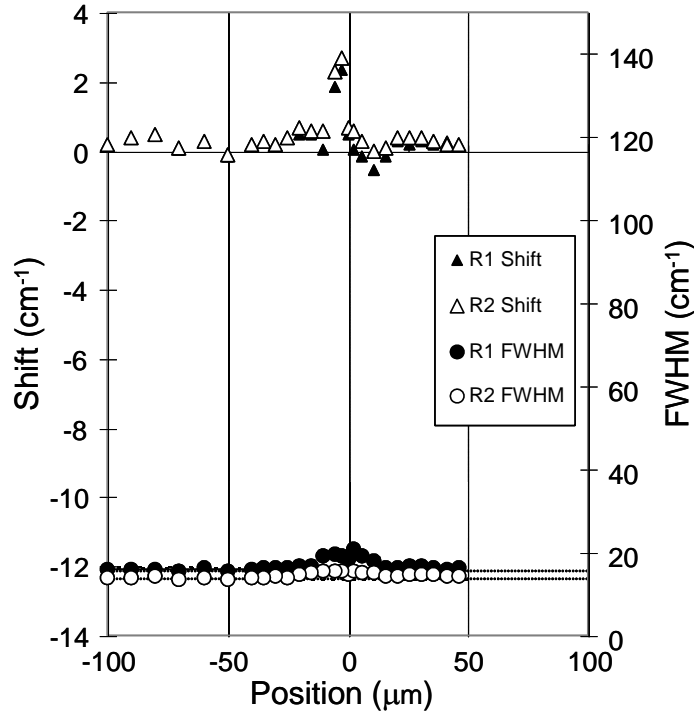


b)

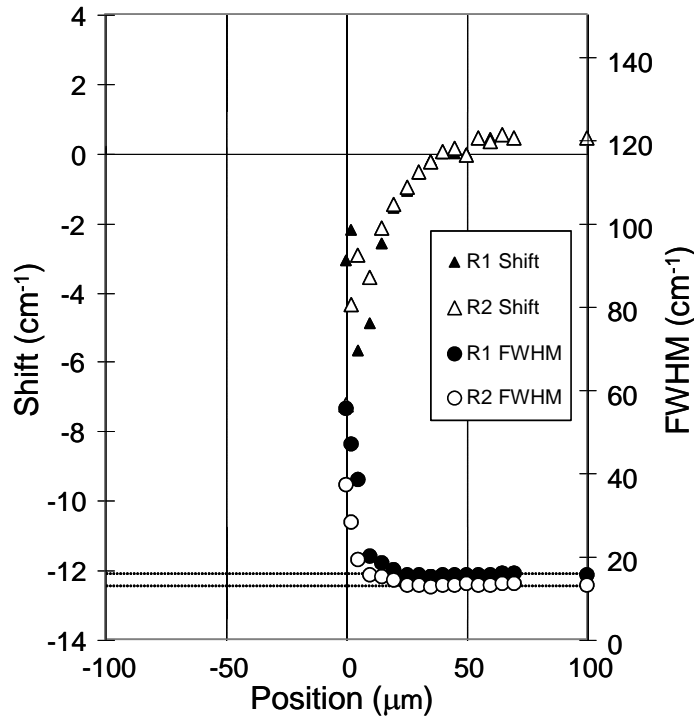
**Figure 2:** Predicted broadening of Cr<sup>3+</sup> fluorescence peaks by dislocations in alumina.

(a) variation of peak broadening with dislocation density, assuming the thickness of dislocated layer is equal to or larger than the illuminated depth;

(b) variation of peak broadening with dislocated layer thickness if the thickness of dislocated layer is less than the illuminated depth, for different dislocation densities; note strong effects are seen only above a critical dislocation density of  $\sim 10^{14} \text{ m}^{-2}$ .



a)



b)

**Figure 3:** Fluorescence peak shift (relative to a strain-free fracture surface) and peak width (full width at half maximum) for R1 and R2 fluorescence lines as a function of position across a 3N indent for (a) alumina, and (b) the x% SiC nanocomposite. The zero position is at the centre of the indent. The horizontal lines represent the average level of FWHM of R1 and R2 lines for the reference fracture surface.

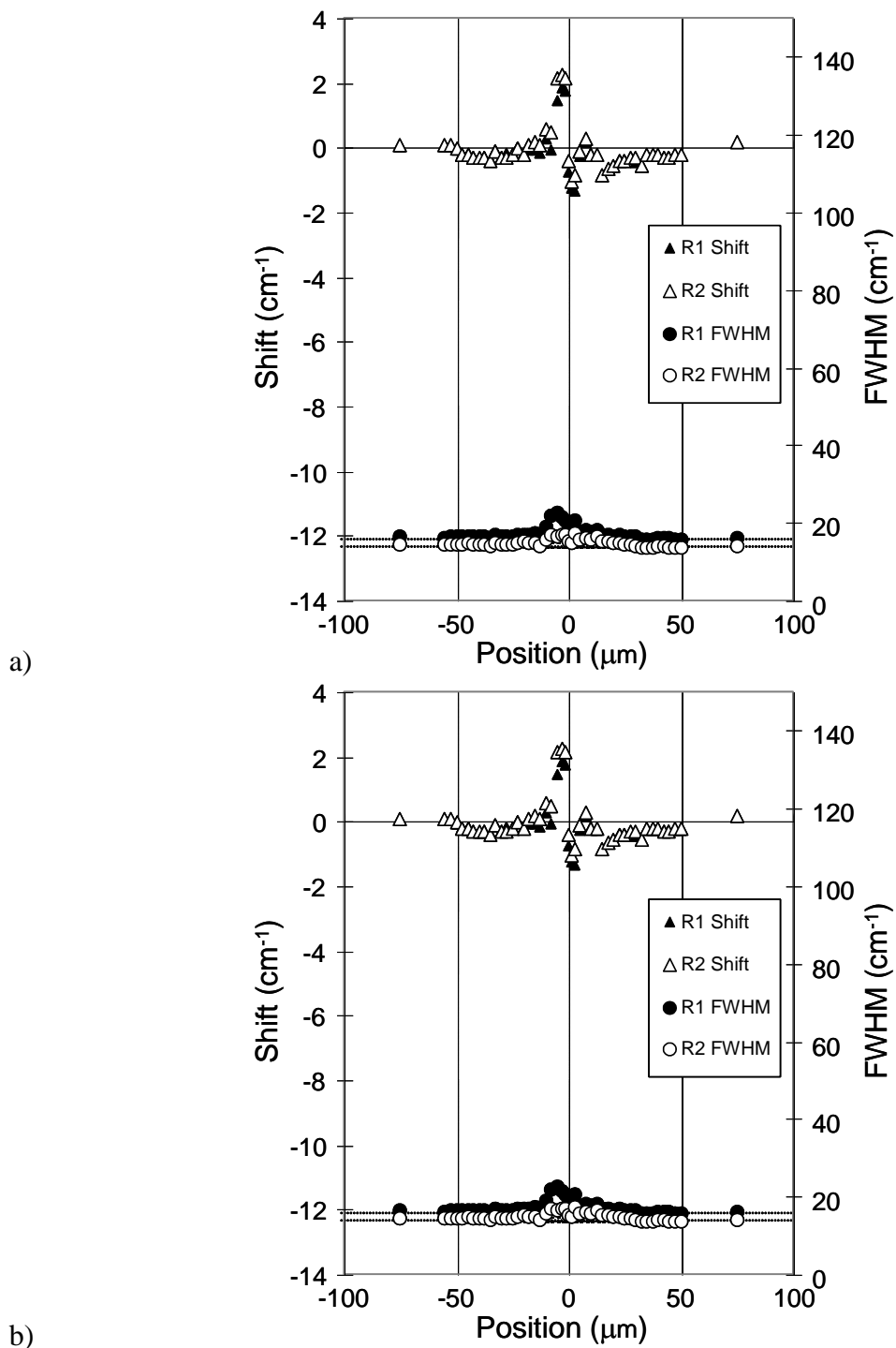


**Figure 4:** Fluorescence peak shift (relative to a strain-free fracture surface) and peak width (full width at half maximum) for R1 and R2 fluorescence lines as a function of position across a 3N scratch for (a) alumina, and (b) the  $x\%$  SiC nanocomposite. The zero position is at the centre of the indent. The horizontal lines represent the average level of FWHM of R1 and R2 lines for the reference fracture surface.



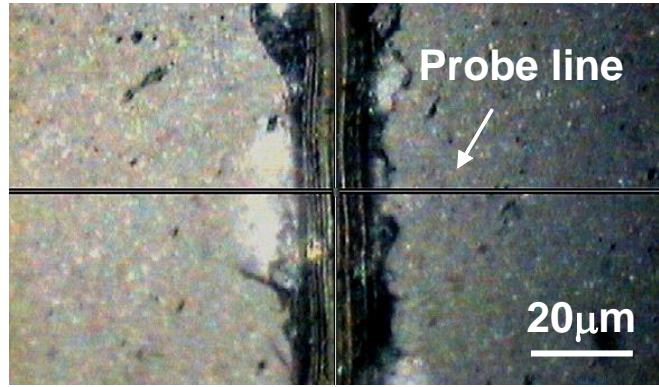


**Figure 5:** Optical microscope image of a 3N scratch in the X% SiC nanocomposite, showing the line across the scratch along which measurements shown in figure 4 were made.

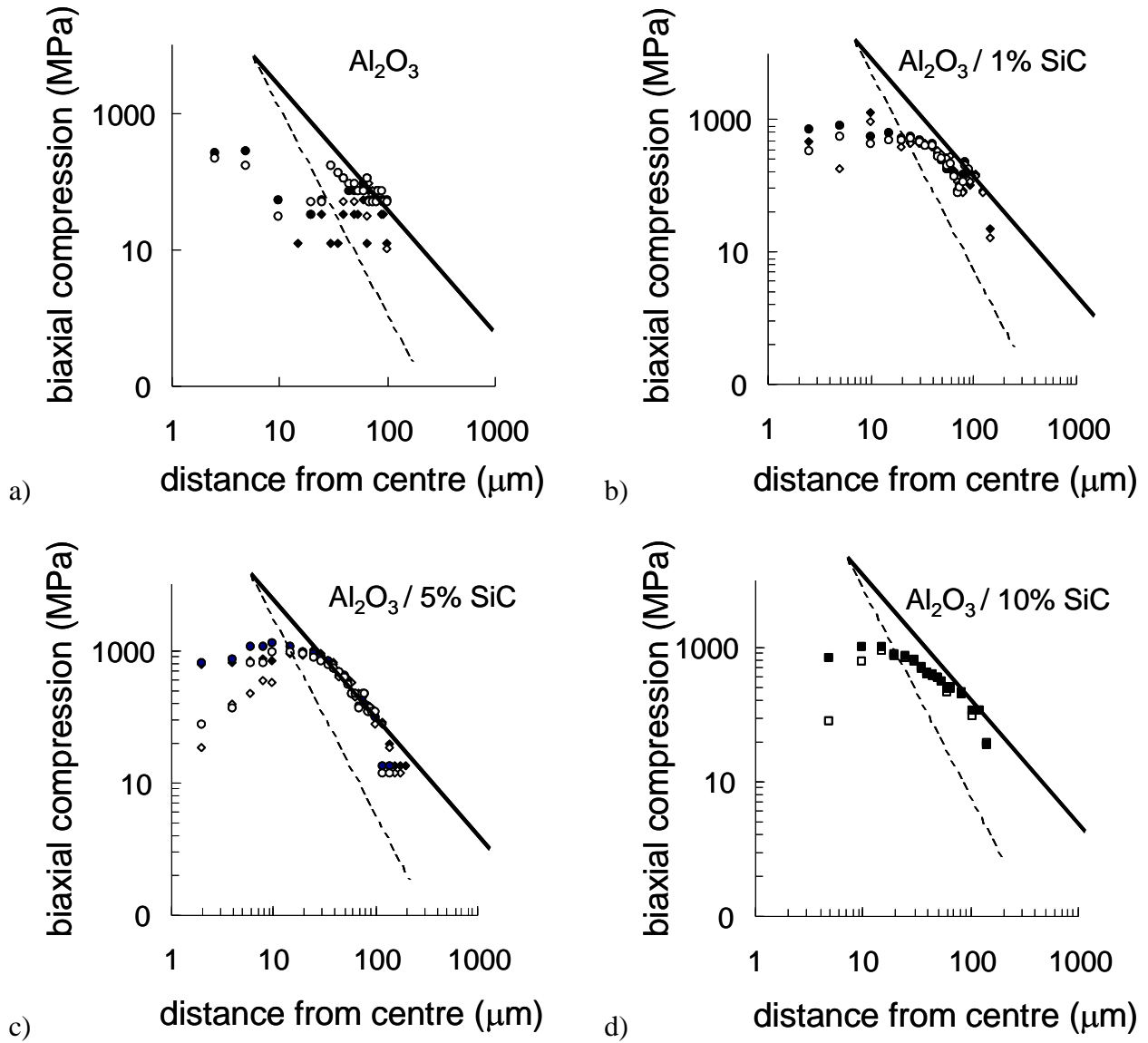


**Figure 6:** Logarithmic plots of residual biaxial compressive stress as a function of distance from the scratch centre (3N load): (a)  $\text{Al}_2\text{O}_3$ ; (b)  $\text{Al}_2\text{O}_3 / 1\text{vol}\% \text{ SiC}$ ; (c)  $\text{Al}_2\text{O}_3 / 5\text{vol}\% \text{ SiC}$ ; (d)  $\text{Al}_2\text{O}_3 / 10\text{vol}\% \text{ SiC}$ . The black line and the dashed line have slopes of -2 and -3 respectively.

**Table 1** Maximum biaxial compressive stresses for indentations and scratches made with various normal loads for alumina and nanocomposites.

Materials	Scratch		Indentation	
	Normal load (N)	Max. stress (MPa)	Normal load (N)	Max. stress (MPa)
Al <sub>2</sub> O <sub>3</sub>	0.5	-89	1	-109
	1	-32	3	-109
	3	-269	5	-267
	5	-466	10	-563
Al <sub>2</sub> O <sub>3</sub> + 1vol%SiC	0.5	-239	1	-318
	1	-694	3	-951
	3	-1227	5	-1603
	5	-1208	10	-1385
Al <sub>2</sub> O <sub>3</sub> + 5vol%SiC	0.5	-245	1	-492
	1	-601	3	-966
	3	-1223	5	-1619
	5	-1717	10	-2132
Al <sub>2</sub> O <sub>3</sub> + 10vol%SiC	0.5	-411	1	-688
	1	-1142	3	-1103
	3	-1024	5	-1518
	5	-1004	10	-1162

**Table 2** Maximum values of fluorescence peak broadening for indentations and scratches made with various normal loads for alumina and nanocomposites.

Materials	SCRATCH		INDENTATION	
	P (N)	$\Delta\text{FWHM}(\text{cm}^{-1})$	P (N)	$\Delta\text{FWHM}(\text{cm}^{-1})$
$\text{Al}_2\text{O}_3$	0.5	2.1	1	1.2
	1	2.5	3	4.9
	3	7.0	5	10.1
	5	8.1	10	16.5
$\text{Al}_2\text{O}_3$ 1vol%SiC	0.5	7.0	1	12.1
	1	11.5	3	29.1
	3	18.3	5	57.9
	5	30.8	10	57.2
$\text{Al}_2\text{O}_3$ 5vl%SiC	0.5	7.9	1	15.2
	1	15.6	3	40.1
	3	24.1	5	60.7
	5	44	10	60.7
$\text{Al}_2\text{O}_3$ 10%SiC	0.5	8.6	1	18.1
	1	20.0	3	10.8
	3	22.9	5	55.4
	5	40.7	10	57.9

$$\Delta\text{FWHM} = \text{FWHM}_{(\text{measured})} - \text{FWHM}_{(\text{reference})}$$